PECVD Synthesis and Thermoelectric Properties of Thin Films of Lead Chalcogenides $(PbTe)_{1-x}(PbS)_x$

Yu. M. Kuznetsov [1*], L. A. Mochalov [1, 2], M. V. Dorokhin [3], D. G. Fukina [4], M. A. Kudryashov [5, 6], Yu. P. Kudryashova [7], A. V. Zdoroveyshchev [8], D. A. Zdoroveyshchev [9], I.L. Kalentyeva [10]

[1] Lobachevsky State University, Nizhny Novgorod, 23 Gagarin Avenue, 603022, Russia
Mail: y.m.kuznetsov@unn.ru

[2] Nizhny Novgorod State Technical University. R.E. Alekseeva, Nizhny Novgorod, 24 Minin street, 603950, Russia mochalov@chem.unn.ru

[3] Lobachevsky State University, Nizhny Novgorod, 23 Gagarin Avenue, 603022, Russia
Mail: dorokhin@nifti.unn.ru

[4] Lobachevsky State University, Nizhny Novgorod, 23 Gagarin Avenue, 603022, Russia
Mail: fukina@ichem.unn.ru

[5] Nizhny Novgorod State Technical University. R.E. Alekseeva, Nizhny Novgorod, 24 Minin street, 603950, Russia kudryashov@phys.unn.ru

[6] Lobachevsky State University, Nizhny Novgorod, 23 Gagarin Avenue, 603022, Russia
Mail: kudryashov@phys.unn.ru

[7] Nizhny Novgorod State Technical University. R.E. Alekseeva, Nizhny Novgorod, 24 Minin street, 603950, Russia
Mail: pjup@mail.ru

[8] Lobachevsky State University, Nizhny Novgorod, 23 Gagarin Avenue, 603022, Russia
Mail: zdorovei@gmail.com

[9] Lobachevsky State University, Nizhny Novgorod, 23 Gagarin Avenue, 603022, Russia
Mail: daniel.zdorov@gmail.com

[10] Lobachevsky State University, Nizhny Novgorod, 23 Gagarin Avenue, 603022, Russia
Mail: kalenteva@nifti.unn.ru

[*]Corresponding author: dorokhin@nifti.unn.ru

Annotation

Lead-based ternary chalcogenide thin films of the $(PbTe)_{1-x}(PbS)_x$ system were obtained by plasma-enhanced chemical vapor deposition technique (PECVD) under conditions of a nonequilibrium low-temperature argon plasma of an RF discharge (40.68

 doi:10.20944/preprints202305.0016.v1

MHz) at a reduced pressure (0.01 Torr). High-purity elements were directly used as starting materials – Pb, S and Te. Plasma-chemical synthesis was carried out on the surface of of c-sapphire and silicon substrate. The physicochemical properties of the films were studied by various analytical methods. The dependence of the Seebeck coefficient, resistivity, and power factor on the structural properties and composition has been studied. The thermoelectric characteristics were found to be dependent on the film composition. Upon the selection of optimal sulfur concentration one can increase the power factor as compared to single phase PbS ot PbTe films.

Key words: lead chalcogenides, thin-film thermoelectric converters, inorganic synthesis, Seebeck coefficient, resistivity, thermoelectric figure of merit, power factor.

1. Introduction

The chalcogenide compounds are multifunctional materials with a number of practical applications. One can mention papers devoted to chalcogenides applications as mid-IR light detectors [1]-[2], photocatalytic materials [3]-[6], and thermoelectric power sources [7]-[10]. The set of the recent papers was devoted to the investigation of thin film lead ternary chalcogenides. The films were obtained by sputter deposition from a solution, physical vapor deposition, molecular beam and liquid phase epitaxy [11]. Among the mentioned techniques the plasma enhanced CVD (PECVD) method is distinguished by some unique capabilities such as possibility of depositing the film on any substrate (unlike epitaxial techniques) and compatibility with the whole set of standard lithography processes [12]. Previously we have demonstrated the applicability of PECVD technique for synthesizing complex chalcogenides [13], [14].

The thermoelectric application of chalcogenides has been the subject of intense investigation since the 1950s [7]. The interest is driven by a unique combination of electrical and thermal properties. Over the past 10 years, the number of publications on this subject has even tripled, for example, [8]-[10]. Thermoelectricity implies conversion of thermal energy into electrical one when creating a temperature gradient (ΔT) on opposite faces of a material. The value of thermo-voltage (U_{TE}) in the case of a linear temperature gradient is given by the expression:

Preprints (www.preprints.org) | NOT PEER-REVIEWED | Posted: 1 May 2023 doi:10.20944/preprints202305.0016.v1

$$U_{TE} = \alpha \cdot \Delta T, \quad (1)$$

where α is a Seebeck coefficient which is a characteristic property of a material. The thermoelectric conversion efficiency is determined by the dimensionless thermoelectric figure of merit (ZT):

$$ZT = \alpha^2 \cdot T/\rho \cdot \lambda, \quad (2)$$

where T is an averaged temperature over the hot and cold faces of the sample, ρ – resistivity, λ is a thermal conductivity.

A number of papers (ex. [15]-[17]) reports that thin films possess lowered thermal conductivity as compared to bulk counterparts. The Seebeck coefficient in thin films is on the contrary lower than that of the bulk analogues. The general mechanism for decrease of α is a decrease of carrier mobility due to greater surface states contribution into carrier scattering. [17]-[19]. However, the thermal conductivity decrease prevails the smaller α allowing one to achieve high values of $ZT > 1$. For that reason, the development of the synthesis technologies for thin film thermoelectric energy converters is considered an urgent task. In particular great success has been achieved within bismuth telluride films, for example, in [20]-[22].

It should be emphasized that the output power of thin-film thermoelectric generator does not exceed the level of μW, thus thin film materials are mostly considered as high-efficiency generators for low-power applications. For a comprehensive description of a thin-film thermoelectric material efficiency, it is preferable to use the power factor (W) along with ZT coefficient:

$$W = \alpha^2/\rho. \quad (3)$$

In the present paper we will mostly focus on investigating power factor W and its' dependence on thin film synthesis parameters.

From the point of view of thermoelectric applications, the most attractive representatives of $A^{IV}B^{VI}$ compounds are PbS, PbSe and PbTe. Those are narrow-gap semiconductors with the bandwidth of 0.39 eV, 0.27 eV and 0.32 eV respectively [23]. Such materials are usually considered as low-temperature thermoelectric converters in the range of up to 500 K. One can cite rather big number of papers devoted to investigation of

Preprints (www.preprints.org) | NOT PEER-REVIEWED | Posted: 1 May 2023 doi:10.20944/preprints202305.0016.v1

thermoelectric properties of either bulk [24]-[25] or thin film [26]-[30] lead chalcogenides. Most recent papers were devoted to studying some approaches to improve the thermoelectric parameters of thin-film PbS or PbTe. Ref. [26] reports on the influence of oxidation on *ZT* value, ref. [29] is devoted to investigation of thickness dependence of the thermoelectric figure of merit. Some progress has been achieved through nanostructuring. For example, paper [27] has demonstrated the enhancement of thermoelectric properties of the films with incorporated PbSe quantum dots. In ref. [30] *ZT* value increase has been shown for the film containing nano-size inclusions of β-PbS_2:Ga phase.

Despite noticeable progress in the development of thermoelectric chalcogenides the practical implementation of such films is very limited. The main direction of further development is the modulation of the phase composition of the material by introducing additional atoms into the crystal lattice. In our previous work [32] we have shown the increase of the power factor for PECVD grown $Pb_{0.05}Se_{0.1}Te_{0.85}/Al_2O_3$ film with respect to $PbTe/Al_2O_3$ system. Similar approach has been discussed in the review paper [33]. The idea was developed towards even more complicated PbTe-PbSe-PbS system. First results for such solutions were demonstrated for bulk nanocomposites with high doping levels [34]. The key feature of composition discussed is the extremely low thermal conductivity due to the mismatch of the phonon spectra of the PbTe and PbS phases. The disadvantage of this approach was the strong carrier scattering at the interphase boundaries which led to a decrease in the Seebeck coefficient and an increase in resistivity. As the result a *ZT* increase was unreasonably insignificant taking into account technological difficulties in the synthesis of a 4-component composition. The most breakthrough thermoelectric characteristics were obtained for $(PbTe)_{z-x}(PbSe)_y(PbS)_x$ pseudo-ternary compounds with high ratio of PbS phase with respect to PbTe [7]-[10]. According to [10] the increase of $(PbSe)_y$ phase content up to $y \sim 0.35$ allows increasing the equilibrium solubility limit of PbS phase in PbTe. This approach had allowed great reduction of the thermal conductivity; however, the abovementioned problem of interfacial carriers scattering causing Seebeck effect decrease was not solved yet.

Next step for improving the thermoelectric characteristics of lead chalcogenides might consist in replacement of PbSe phase by Pb-S-Te compounds. Such compounds are

Preprints (www.preprints.org) | NOT PEER-REVIEWED | Posted: 1 May 2023 doi:10.20944/preprints202305.0016.v1

poorly discussed in the literature. One can cite only few publications, for example, one devoted to investigation of mechanical properties of bulk PbS_xTe_{1-x} [35]. The thermoelectric properties of such compounds weren't investigated neither for bulk nor for thin film materials to the best of our knowledge. The purposes of this work are to propose a new approach to the synthesis of $(PbTe)_{1-x}(PbS)_x$ ternary lead chalcogenides and to establish the relationship between the growth parameters and thermoelectric properties of these materials.

2. Materials and methods

A sketch of the experimental PECVD system is shown in Figure 1, the principle of operation of the set-up was described in detail in [13], [14].

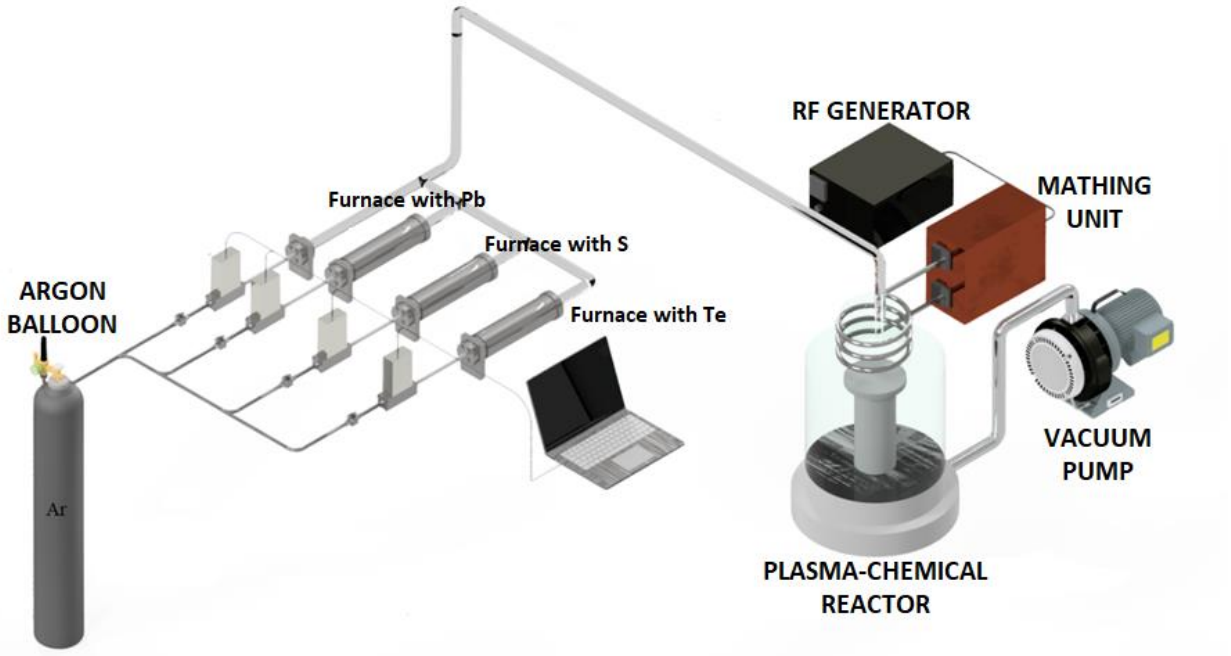

Figure 1. Schematic of the plasma enhanced CVD synthesis set-up

The initial high-purity lead and chalcogens were loaded into quartz evaporators equipped with an external heater and a thermocouple for temperature control. Plasma-forming gas (Ar) was passed at a constant rate through evaporators heated above the melting point of the precursors loaded. The gas flow was set with high precision using gas flow controllers. The amount and ratio of the reagents supplied to the plasma discharge were kept constant during the experiments. The deposition of $(PbTe)_{1-x}(PbS)_x$ films was carried out in following conditions: lead source temperature – 700 °C, sulfur temperature –

Preprints (www.preprints.org) | NOT PEER-REVIEWED | Posted: 1 May 2023 doi:10.20944/preprints202305.0016.v1

130 °C, tellurium temperature – 440 °C, total pressure in the reactor – 0.01 Torr, total flow rate – 30 ml/min. The ratio of sulfur and tellurium in the grown films was controlled by changing the discharge power (60 W and 100 W). The silicon (100) and c-sapphire (100) substrates with the size of 10×10×1 mm^3 were used for film deposition. A selection of sapphire substrates was motivated by the task of separate consideration of $(PbTe)_{1-x}(PbS)_x$ thermoelectric properties. The sapphire substrate is highly resistive thus making no contribution neither into entire system conductivity nor into the Seebeck coefficient. Low thermal conductivity of sapphire makes it possible to create sufficient values of the temperature gradient without the use of special tools for supplying and removing heat flux.

The chemical composition study of the fabricated samples was carried out by X-ray microanalysis using an X-MaxN 20 (Oxford Instruments) energy dispersive elemental analysis setup implemented on the basis of JSM IT-300LV scanning electron microscope (JEOL). The measurements were carried out under conditions of high vacuum and accelerating voltage of 20 kV. The Seebeck coefficient was measured upon the controlled generation of a temperature gradient (ΔT) on the edges of the structure under study. The sample was placed on two independent graphite stoves (heater), the heating of each was controlled independently by K-type control thermocouples, which were connected to the TRM101-PID controllers (Figure 2). The free ends of the thermocouples were thermostatted in a vacuum connector with a stabilized temperature T_{room}.

The K-type measuring thermocouples (Ch_i, A_i) attached on top of the structures were used to record the resulting distribution of the thermal field. Within the measurement process the thermoelectric signal was recorded by measuring the voltage between the legs of chromel (U_{Ch1}) and alumel (U_{A1}), this allowed getting rid of the parasitic contributions into the thermoelectric signal (Figure 2a). In order to take the asymmetry of the thermal contact between the tables into account, a same gradient of $-\Delta T$ was created in the opposite direction, and corresponding values of the thermopower U_{Ch2} and U_{A2} were recorded (Figure 2b). The entire registration process was carried out in automatic mode using the L-CARD E14-140-MD data collection system. The measurement error of the Seebeck coefficient is ~ 5 %. Detailed information on the Seebeck coefficient measurement can be found in [17], [18], [32].

Preprints (www.preprints.org) | NOT PEER-REVIEWED | Posted: 1 May 2023 doi:10.20944/preprints202305.0016.v1

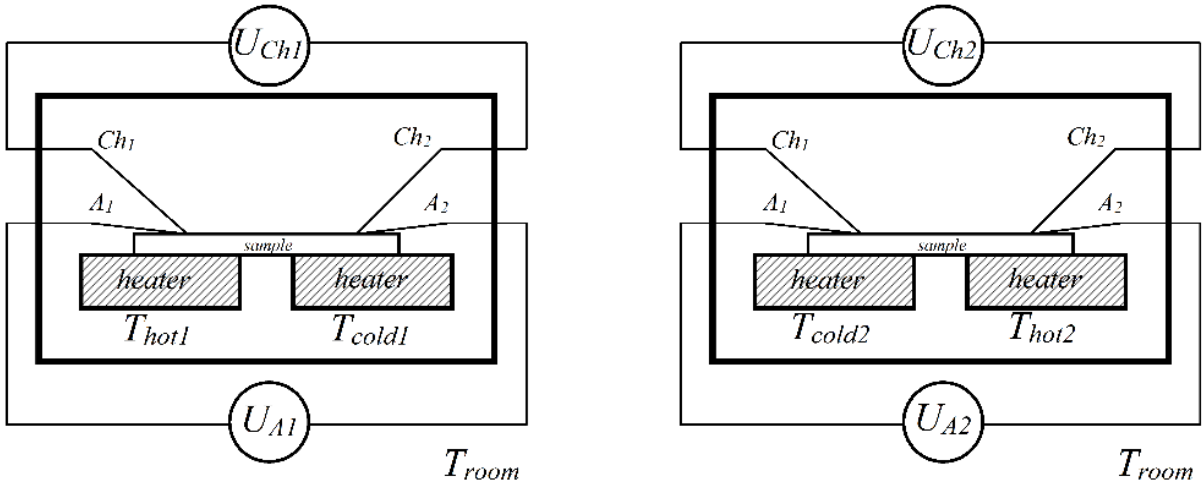

a b

Figure 2. Seebeck coefficient measurement scheme

The electrical resistance of the investigated thin films was also recorded by measuring the I-V characteristic with a classical two-contact circuit. Resistance recording was carried out upon keeping the temperatures of two stages equal. More details on the technique can be found in [17], [18], [36]. The measurement error for resistivity is ~ 1 %.

The measurements of Seebeck coefficient and resistivity were carried out in the temperature range of 50-275 °C. The power factor was calculated by formula (3). Power factor calculation error was ~ 10 %.

The concentration of carriers was measured by recording the magnetic field dependence of the Hall resistance. During these measurements a sample was placed into a magnetic field induced by an electromagnet. An electric current was passed through the sample and the Hall resistance was recorded using a Keithley-2401 current source and voltage meter. The magnetic field was measured using an InSb-based Hall sensor using an L-Card E14-140MD data acquisition system. The measurements were carried out at 300 K. The concentration and mobility calculation error was ~ 3 %.

3. Results and discussion

3.1. Elemental analysis and scanning electron microscopy

The surface of all $(PbTe)_{1-x}(PbS)_x$ samples was uniform, matte and gray. An increase in the sulfur content was accompanied by a change in the surface shade from dark gray to

Preprints (www.preprints.org) | NOT PEER-REVIEWED | Posted: 1 May 2023 doi:10.20944/preprints202305.0016.v1

light gray (silver). The average layer thickness was 400-600 nm in case an average deposition time of 1 hour.

Table 1 presents the results of X-ray microanalysis of thin film samples depending on the plasma power and the type of substrate used. As can be seen from the data presented in Table 1 both the plasma power and the substrate material affect the macrocomposition of the fabricated films. An increase of the discharge power from 60 to 100 W leads to increase in the sulfur content and, accordingly, to a decrease in the tellurium content. The S content increases from 3 to 10 at.% for sapphire substrate and from 5 to 12 at.% for silicon substrate. Thus, samples grown on a silicon substrate include some higher ratio of sulfur compared to films grown under similar conditions on sapphire (with respect to the accuracy of the analytical method).

Table 1. Synthesis conditions and film compositions $(PbTe)_{1-x}(PbS)_x$

№	*P* (W)	Substrate	Compound, at. %			
			Pb	S	Te	
1	60	Al_2O_3	50±1	3±1	47±1	$(PbTe)_{0.94}(PbS)_{0.06}$
2	60	Si	50±1	5±1	45±1	$(PbTe)_{0.90}(PbS)_{0.10}$
3	100	Al_2O_3	50±1	10±1	40±1	$(PbTe)_{0.80}(PbS)_{0.20}$
4	100	Si	50±1	12±1	38±1	$(PbTe)_{0.76}(PbS)_{0.24}$

Figures 3a-d show scanning electron microscopy images of $(PbTe)_{1-x}(PbS)_x$ films on silicon and sapphire substrates. Grains with sharply defined edges are evenly distributed over the surface on all lead-based ternary chalcogenide films. It should be emphasized that neither defects like cracks, detachments or point holes were revealed in the films. The presented SEM images allow drawing a conclusion that the synthesized materials are polycrystalline, while the morphology of the resulting structures is affected by both the plasma power and the substrate material.

With the plasma power increase, the average grain size decreases from 1 μm to 500 nm in the case of a sapphire substrate (Figure 3a-b correspondingly) and from 2 μm to 1 μm in the case of silicon substrates (Figure 3c-d).

Preprints (www.preprints.org) | NOT PEER-REVIEWED | Posted: 1 May 2023 doi:10.20944/preprints202305.0016.v1

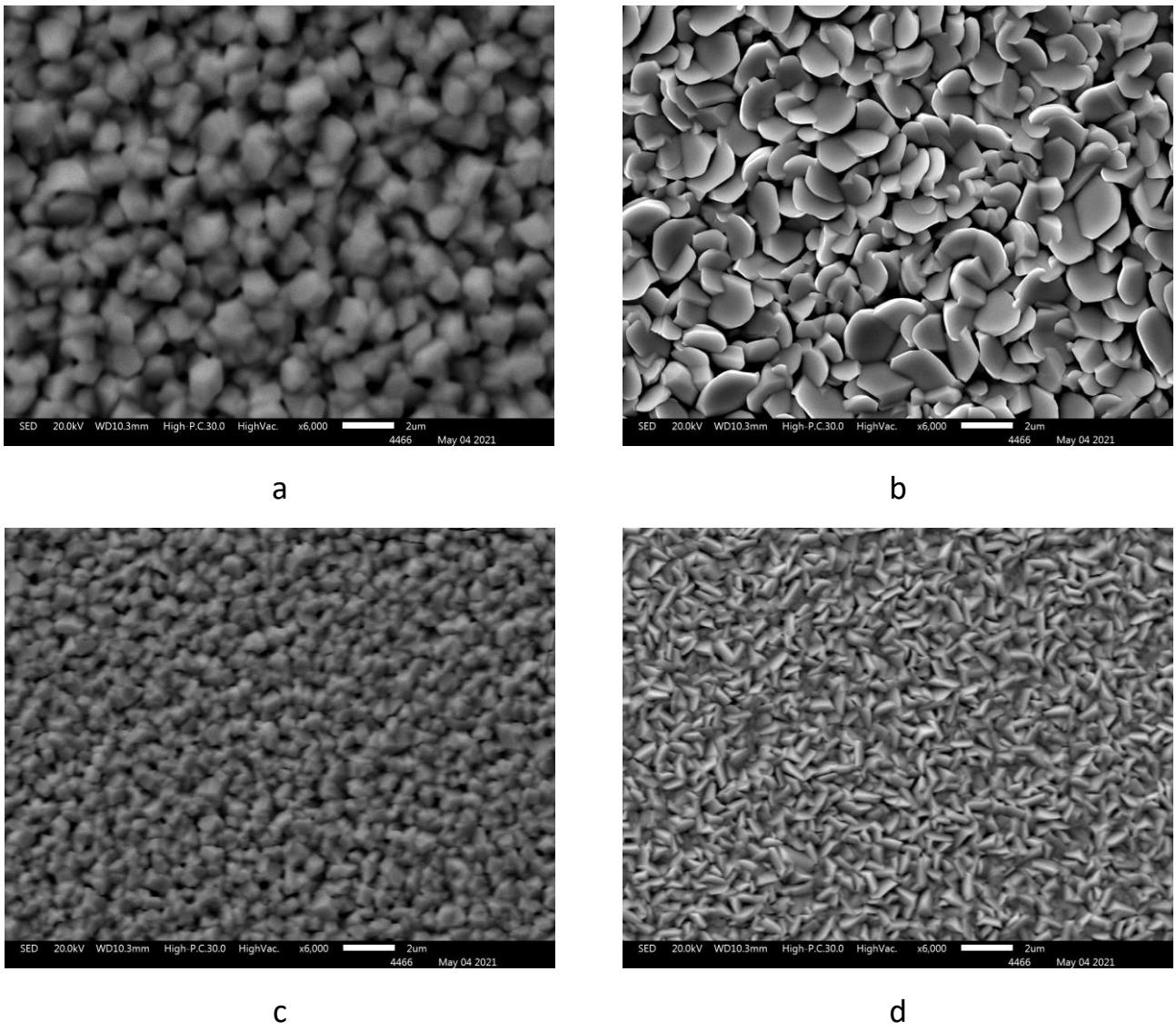

Figure 3. SEM images of $(PbTe)_{1-x}(PbS)_x$ films of various compositions: sample 1 (a), sample 2 (b), sample 3 (c), sample 4 (d)

3.2. Results of XRD phase analysis

Figure 4b shows a distinctive XRD pattern for films of the $(PbTe)_{1-x}(PbS)_x$ system. The films represent a two-phase system containing PbS and PbTe phases. To confirm this conclusion, the figure 4 shows the XRD curves for pure PbS (Figure 4a) and PbTe (Figure 4c).

The orientation of lead telluride crystallites in the (200) direction remained unchanged after small amount of sulfur was introduced. On the contrary, a high tellurium content (x = 0.06) has led to a change in the preferred PbS crystallites orientation from (111) for pure lead sulfide to (311) for $(PbTe)_{1-x}(PbS)_x$ films. The calculated lattice constants of PbS and PbTe were approximately 5.93 and 6.46 Å, respectively.

Preprints (www.preprints.org) | NOT PEER-REVIEWED | Posted: 1 May 2023 doi:10.20944/preprints202305.0016.v1

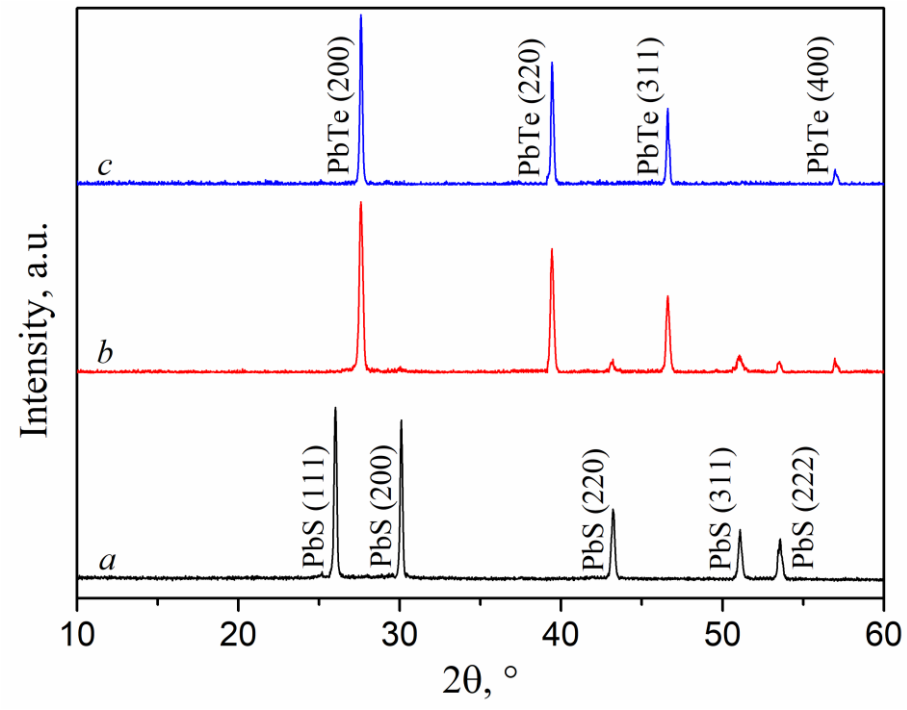

Figure 4. XRD curves of $(PbTe)_{1-x}(PbS)_x$ films on sapphire of various compositions: a – PbS, b – $(PbTe)_{0.94}(PbS)_{0.06}$, c – PbTe

These values are consistent with literature data; moreover they remain unchanged regardless of a film composition. In addition, the PbTe phase was subjected to a decrease in the size of crystallites, an increase in the density of dislocations, and microdeformations upon the introduction of either tellurium into lead sulfide or sulfur into lead telluride. In particular, the crystallite size was decreased from about 45 to 30 nm, the dislocation density was increased from 0.48×10^{15} to 0.97×10^{15} m^{-2}, and the microdeformation was increased from 0.0071 to 0.0101. In case of PbS phase the reliable estimation of the crystallites' parameters turned out to be complicated because of very low intensity of the reflections observed. However, estimation of the (311) reflection half-width allows assuming that the crystallite size was also decreased.

The effect of the substrate type on the diffraction patterns of $(PbTe)_{1-x}(PbS)_x$ films is shown in Figure 5a,b. For both substrates under study, a two-phase system consisting of PbS and PbTe was revealed. However, in the case of sapphire substrate, PbTe crystallites were predominantly oriented in the (200) direction, while for a film deposited on silicon, the (220) direction was dominant (figure 5b). Another peculiarity revealed was a shift of the diffraction maxima from PbTe towards larger angles detected for the film grown on silicon substrate. Such shift indicates the compression of the crystal lattice of lead telluride

Preprints (www.preprints.org) | NOT PEER-REVIEWED | Posted: 1 May 2023 doi:10.20944/preprints202305.0016.v1

in comparison with the film grown on sapphire. The calculated lattice constants of crystallites in PbTe films deposited on sapphire and silicon were 6.46 and 6.44 Å, respectively. The lattice parameter of PbS crystallites and their preferred orientation were on the contrary found to be independent on a substrate type. Finally, the sizes of crystallites of both phases were slightly higher in films grown on the silicon substrate.

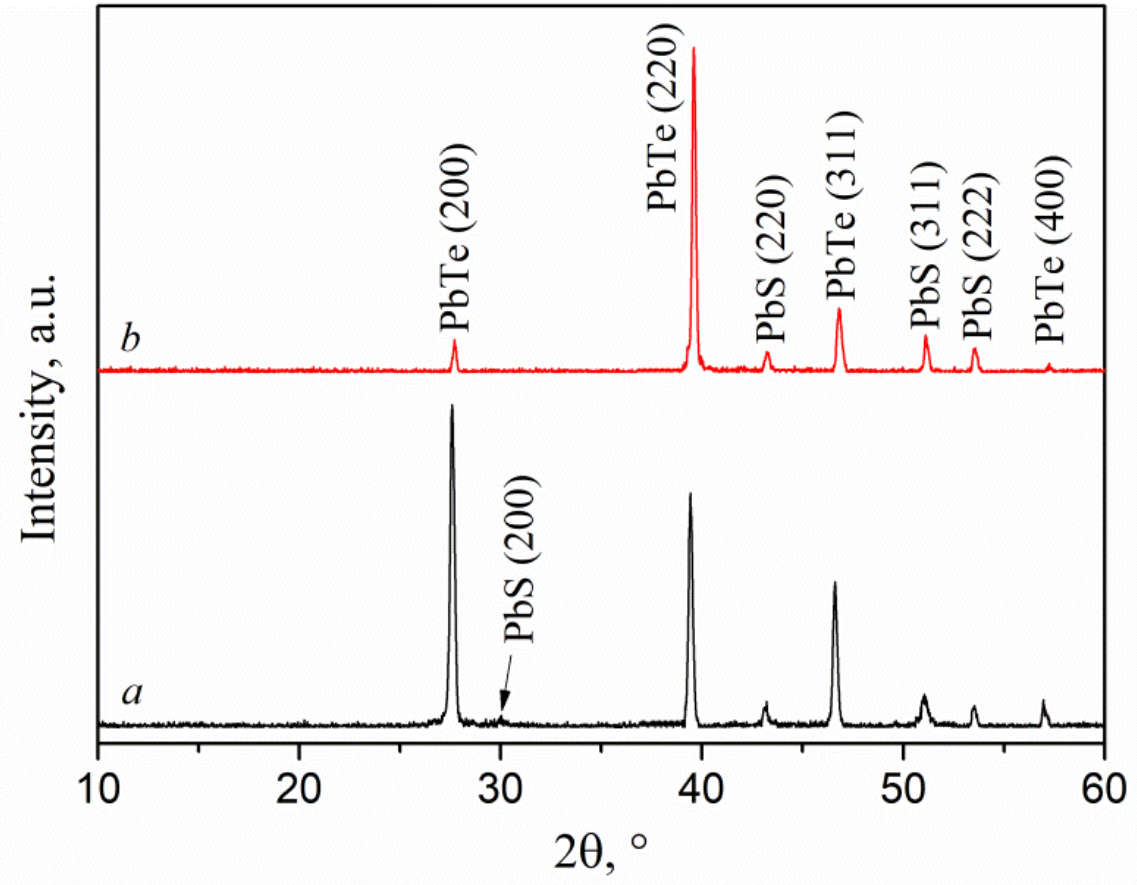

Figure 5. XRD curves of $(PbTe)_{1-x}(PbS)_x$ films deposited on sapphire with x = 0.06 (a) and silicon with x = 0.1 (b)

3.3. Thermoelectric properties of the films

One important condition for investigating the transport and thermoelectric characteristics of thin-film samples is negligible electrical conductivity of the substrate. Otherwise, due to a much greater thickness as compared to the film, the substrate can make a decisive contribution to the properties under study [18]. In the case of a silicon substrate, shunting of the thin-film layer upon heating is unavoidable. For this reason, the thermoelectric properties will be further considered only for the films grown on sapphire.

Preprints (www.preprints.org) | NOT PEER-REVIEWED | Posted: 1 May 2023 doi:10.20944/preprints202305.0016.v1

A series of samples with the sulfur content varied from 0 at.% to 15 at.% was fabricated. The list of the investigated samples is presented in Table 2.

Table 2. List of studied films grown on sapphire with indication of transport parameters at T = 300 K

№	Состав	ρ, мкОм·м	μ, см^2/В·с	p, 10^{18} см$^{-3}$
1	PbTe	627±6	150±5	0.67±0.02
2	$(PbTe)_{0.9}(PbS)_{0.1}$	332±3	72.6±2.2	2.59±0.08
3	$(PbTe)_{0.8}(PbS)_{0.2}$	200±2	50.3±1.5	6.21±0.19
4	$(PbTe)_{0.7}(PbS)_{0.3}$	176±2	49.2±1.5	7.22±0.22

The mobility and concentration of carriers in the films under study were calculated from the magnetic field dependence of the Hall resistance (Table 2). The film thickness was estimated from atomic force microscopy by measuring the step height at the boundary of the sapphire surface covered and uncovered with a film. Such a step is usually formed within the film growth process since the material is not being deposited on the area shadowed by a substrate holder. The measured thickness of the films was 0.5 ± 0.1 μm.

From the magnetic field dependence of the Hall Effect, it was found that all films were *p*-type conductivity. From the data in Table 2 it can be seen that the introduction of sulfur lead to a decrease in the resistivity of the film. An increase in the sulfur concentration is accompanied with an increase in the carrier concentration. The carrier mobility in sample 1 significantly exceeds the values obtained for samples 2–4, which is associated with additional carriers' scattering at interfaces.

The measured temperature dependences of resistivity and Seebeck coefficient are shown in Figures 6a and 6b, respectively. The measured values were used to calculate the temperature dependences of a power factor (figure 6c). From the temperature dependence of resistivity (figure 6a) it can be seen that all structures demonstrated a semiconductor nature of conductivity – i.e. the resistance decreased with increasing temperature. A maximum on a temperature dependence of Seebeck coefficient at the temperature range of 75-175 °C was revealed for the entire batch.

Preprints (www.preprints.org) | NOT PEER-REVIEWED | Posted: 1 May 2023 doi:10.20944/preprints202305.0016.v1

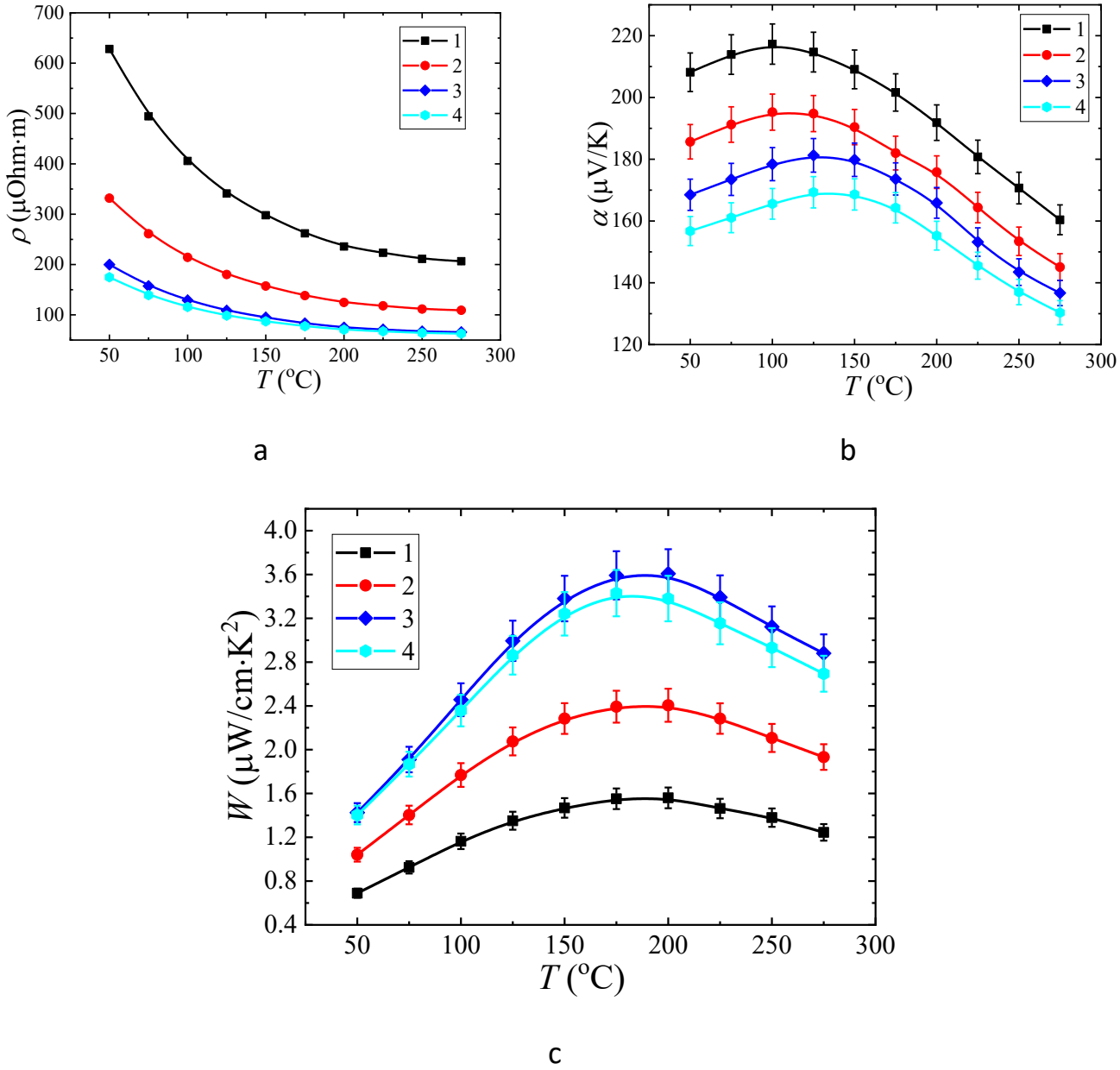

Figure 6. Experimentally obtained temperature dependences of: resistivity (a), Seebeck coefficient (b), power factor (c)

The value of the Seebeck coefficient was positive over the entire measured temperature range. This is consistent with the *p*-type conductivity revealed from the Hall effect measurement. The decrease in the Seebeck coefficient at high temperatures is associated with an increased contribution of intrinsic conductivity. The absolute values of the Seebeck coefficient correlate well with the resistivity value for all samples. For example, sample 1, possessing the highest resistivity among the batch (figure 6a line 1) demonstrated the highest value of the Seebeck coefficient in the entire temperature range (figure 6b line 1). In the sample 4, the lowest resistivity was accompanied with the lowest

Preprints (www.preprints.org) | NOT PEER-REVIEWED | Posted: 1 May 2023 doi:10.20944/preprints202305.0016.v1

Seebeck coefficient (figure 6a and 6b correspondingly). The resistivity was found to depend nonmonotonically on the sulfur content in the films. Sulfur content increase from 0 at.% (sample 1) to 5 at.% (sample 2) lead to a sharp decrease in resistivity (figure 6a, lines 1 and 2). Further increase of sulfur content to 15 at.% lead to much smaller decrease of a resistivity (figure 6a, lines 3 and 4).

A similar behavior was revealed for the temperature dependence of the Seebeck coefficient (figure 6b). We should note that the sulfur content has also affected the position of Seebeck coefficient maximum on the temperature dependence. In the sample 1 the maximal Seebeck coefficient was obtained at 100 ^{o}C (figure 6a line 1), in the sample 4 – maximum point was 150 ^{o}C (figure 6a line 4). Such shift is attributed to the increasing contribution of PbS phase into the current transfer through the film. It is known from [23] that the PbS bandgap is by 70 meV higher than that of PbTe. Thus PbS incorporation into PbTe has allowed not only increasing the thermoelectric power factor but also shifting the operating temperature range towards higher temperatures.

The highest power factor value of $W \sim 3.6$ μW/cm^2·K was obtained in sample 3, that includeed 10 at.% of sulfur (figure 6d line 3). The obtained maximum value of the power factor exceeds the values reported in [32]. The decrease of a sulfur content to 5 at.% in Sample 2 lead to decrease of a power factor as compared to 10 at.% sample. The Seebeck coefficient increase (Figure 6a line 2) was fully compensated by great increase of a resistivity (Figure 6d line 2). Single phase PbSe Sample 1 was characterized by the lowest power factor among the batch (figure 6d line 1) which was due to a greatly increased resistivity value (figure 6a line 1). Thus, it is shown that a two-phase thin film can possess enhanced thermoelectric characteristics as compared to a homogeneous single-phase film, despite the additional role of interfacial carrier scattering. Even greater increase of a sulfur content up to 15 at.% allowed for further decrease of the resistivity (figure 6a line 4). However this was accompanied by even greater reduction of a Seebeck coefficient (figure 6b line 4), which in total lead to a power factor decrease (figure 6d line 4). A decrease in mobility and an increase in the carrier concentration can also be noted (Table 2). Therefore, there is an optimum sulfur concentration that allows achieving the highest

 doi:10.20944/preprints202305.0016.v1

power factor values. A further optimization of thermoelectric figure of merit in such films can be achieved introduction of a dopant.

4. Conclusions

The semiconductor $(PbTe)_{1-x}(PbS)_x$ layers have been grown of sapphire and silicon substrates. Structural investigation of the fabricated layers was carried out. The features of $(PbTe)_{1-x}(PbS)_x$ film growth on sapphire substrates were shown, in particular the investigation of the temperature dependences of thermoelectric properties of the films was carried out. A strong influence of the stoichiometric composition on the type of structure and the value of thermoelectric properties, and in particular, the power factor, was shown.

5. Acknowledgements

The work was supported by the Ministry of Science and Higher Education of the Russian Federation [FSWR-2023-0024].

X-ray microanalysis and scanning electron microscopy were performed using the equipment of the Center for Collective Usage "New Materials and Resource-Saving Technologies" (Research Institute of Chemistry, Lobachevsky State University of Nizhny Novgorod).

References

[1] Wang, B.; Zhong, S.P.; Zhang, Z.B.; Zheng, Z.Q.; Zhang, Yu.P.; Zhang, H. Broadband photodetectors based on 2D group IV_A metal chalcogenides semiconductors. *Appl. Mater. Today*. **2019**, 15, 115-138.

[2] Xu, Y.; Li, R.; Bai, S.; Li, Y.; Jia, Z.; Yang, Yu.; Cui, E.; Yao, F.; Wang, D.; Lei, C.; Lin, Q. Chalcogenide-based narrowband photodetectors for imaging and light communication. *Adv. Funct. Mater.* **2022**, 33, 2212523.

[3] Tayyab, M.; Liu, Yu.; Liu, Z.; Xu, Z.; Yue, W.; Zhou, L.; Lei, J.; Zhang, J. A new breakthrough in photocatalytic hydrogen evolution by amorphous and chalcogenide enriched cocatalysts. *Chem. Eng. J.* **2023**, 455, 140601.

[4] Tshimangadzo, S.M.; Philiswa, N.N. Review on metal chalcogenides and metal chalcogenide-based nanocomposites in photocatalytic applications. *Chem. Afr.* **2023**, 19, e01509.

 doi:10.20944/preprints202305.0016.v1

[5] Ali, S.A.; Ahmad, T. Chemical strategies in molybdenum based chalcogenides nanostructures for photocatalysis. *Int. J. Hydrog. Energy* **2022**, 47, 29255-29283.

[6] Li J.; Jimenez-Calvo, P.; Paineau, E.; Ghazzal, M.N. Metal chalcogenides based heterojunctions and novel nanostructures for photocatalytic hydrogen evolution. *Catalysts* **2020**, 10, 89.

[7] Yamini, S.A.; Wang, H.; Gibbs, Z.M.; Pei, Y.; Dou, S.X.; Snyder, G.J. Chemical composition tuning in quaternary p-type Pb-chalcogenides – a promising strategy for enhanced thermoelectric performance. *Phys. Chem. Chem. Phys.* **2014**, 16, 1835-1840.

[8] Yamini, S.A.; Wang, H.; Gibbs, Z.M.; Pei, Y.; Mitchell, D.R.G.; Dou, S.X.; Snyder, G.J. Thermoelectric performance of tellurium-reduced quaternary p-type lead–chalcogenide composites. *Acta Mater*. **2014**, 80, 365-372.

[9] Yamini, S.A.; Patterson, V.; Santos, R. Band-gap nonlinearity in lead chalcogenide (PbQ, Q = Te, Se, S) alloys. *ACS Omega*. **2017**, 2, 3417-3423.

[10] Manettas, A; Santos, R.; Ferreres, X.R.; Yamini, S.A. Thermoelectric performance of single phase p-type quaternary $(PbTe)_{0.65-x}(PbSe)_{0.35}(PbS)_x$ alloys. *ACS Appl. Energy Mater*. **2018**, 1, 1898-1903.

[11] Hone, F.G.; Ampong, F.K.; Nkum, R.K.; Boakye, F. Band gap engineering in lead sulphur selenide ($PbS_{1-x}Se_x$) thin films synthesized by chemical bath deposition method. *J Mater Sci: Mater Electron*. **2017**, 28, 2893-2900.

[12] Kudryashov, M; Mochalov, L.; Nezdanov, A.; Kornev, R.; Logunov, A.; Usanova, D.; Mashin, A.; De Filpo, G.; Gogova, D.; A novel plasma-based method for synthesis of As-Se-Te films: impact of plasma parameters on the structure, composition, and optical properties. *Superlattices Microstruct.* **2019**, 128, 334-341.

[13] Mochalov, L.; Logunov, A.; Prokhorov, I.; Sazanova, T.; Kudrin, A.; Yunin, P.; Zelentsov, S.; Letnianchik, A.; Starostin, N.; Boreman, G.; Vorotyntsev, V. Plasma-chemical synthesis of lead sulphide thin films for near-IR photodetectors. *Plasma Chem. Plasma Process*. **2020**, 41, 493.

[14] Mochalov, L.; Logunov, A.; Markin, A.; Kitnis, A.; Vorotyntsev, V. Characteristics of the Te-based chalcogenide films dependently on the parameters of the PECVD process. *Opt. Quantum Electron*. **2020**, 52, 197.

 doi:10.20944/preprints202305.0016.v1

[15] Kumanek, B.; Janas, D. Thermal conductivity of carbon nanotube networks: a review. *J. Mater. Sci*. **2019**, 54, 7397-7427.

[16] Tambasov, I.A.; Voronin, A.S.; Evsevskaya, N.P.; Kuznetsov, Yu.M.; Luk'yanenko, A.V.; Tambasova, E.V.; Gornakov, M.O.; Dorokhin, M.V.; Loginov, Yu.Yu. Experimental study of the thermal conductivity of single-walled carbon nanotube-based thin films. *Phys. Solid State*. **2020**, 6, 1090-1094.

[17] Dorokhin, M.V.; Kuznetsov, Yu.M.; Lesnikov, V.P.; Zdoroveishchev, A.V.; Demina, P.B.; Erofeeva, I.V. Studies of thermoelectric properties of superlattices based on manganese silicide and germanium. *Phys. Solid State*. **2019**, 12, 2348-2352.

[18] Erofeeva, I.V.; Dorokhin, M.V.; Lesnikov, V.P.; Kuznetsov, Yu.M.; Zdoroveyshchev, A.V.; Pitirimova, E.S. Thermoelectric effects in nanoscale layers of manganese silicide. *Semiconductors*. **2017**, 11, 1403-1408.

[19] Orlova, D.S.; Rogacheva, E.I. Galvanomagnetic properties of thin films of bismuth, doped with tellurium. *Nanosyst. Nanomater. Nanotechnologies*. **2009**, 2, 487-493. (in Russian).

[20] Park, N-W.; Lee, W-Y.; Yoon, Y-S.; Kim, G-S.; Yoon, Y-G.; Lee, S-K. Achieving out-of-plane thermoelectric figure of merit ZT = 1.44 in a p-type $Bi_2Te_3/Bi_{0.5}Sb_{1.5}Te_3$ superlattice film with low interfacial resistance. *ACS Appl. mater. interfaces*. **2019**, 11, 38247-38254.

[21] Zheng, Z-H.; Shi, X-L.; Ao, D-W.; Liu, W-D.; Li, M.; Kou, L-Z.; Chen, Y-X.; Li, F.; Wei, M.; Liang, G-X.; Fan, P.; Lu, G.Q.M.; Chen, Z-G. Harvesting waste heat with flexible Bi_2Te_3 thermoelectric thin film. *Nat. Sustain*. **2022**, 6, 180-191.

[22] Zheng, D.; Jin, H.; Liao, Y.; Ji, P. Bi_2Te_3 nanowires tuning PEDOT:PSS structure for significant enhancing electrical transport property. *Mater. Lett*. **2023**, 338, 134019.

[23] Lach-hab, M.; Papaconstantopoulos, D.A.; Mehl, M.J. Electronic structure calculations of lead chalcogenides PbS, PbSe, PbTe. *J. phys. solids*. **2002**, 63, 833-841.

[24] Pei, Ya.; LaLonde, A.; Iwanaga, S.; Snyder, G.J. High thermoelectric figure of merit in heavy hole dominated PbTe. *Energy Environ. Sci*. **2011**, 4, 2085-2089.

[25] Heremans, J.P.; Jovovic, V.; Toberer, E.S.; Saramat, A.; Kurosaki, K.; Charoenphakdee, A.; Yamanaka, S.; Snyder, G.J. Enhancement of thermoelectric

efficiency in PbTe by distortion of the electronic density of states. *Science*. **2008**, 321, 554-557.

[26] Rogacheva, E.I.; Krivulkin, I.M.; Nashchekina, O.N.; Sipatov, A.Yu.; Volobuev, V.V. Effect of oxidation on the thermoelectric properties of PbTe and PbS epitaxial films. *Appl. Phys. Lett*. **2001**, 78, 1661-1663.

[27] Yang, D.; Lu, C.; Yin, H.; Herman, I.P. Thermoelectric performance of PbSe quantum dot films. *Nanoscale*. **2013**, 5, 7290-7296.

[28] Yan, Q.; Chen, H.; Zhou, W.; Hng, H.H. Boey, F.Y.C.; Ma, J. A simple chemical approach for PbTe nanowires with enhanced thermoelectric properties. *Chem. Mater*. **2008**, 20, 6298-6300.

[29] Rogacheva, E.I.; Nashchekina, O.N.; Vekhov, Y.O.; Dresselhaus, M.S.; Cronin, S.B. Effect of thickness on the thermoelectric properties of PbS thin films. *Thin Solid Films*. **2003**, 423: 115-118.

[30] Geethu, R.; Jacob, R.; Shripathi, T.; Okram, G.S.; Ganesan, V.; Tripathi, S.; Fatima, A.; Sreenivasan, P.V.; Urmila, K.S.; Pradeep, B.; Philip, R.R. Optoelectronic and thermoelectric properties in Ga doped β-PbS_2 nanostructured thin films. *Appl. Surf. Sci*. **2012**, 258, 6257-6260.

[31] Sun, J.; Yeh, M-L.; Jung, B.J.; Zhang, B.; Feser, J.; Majumdar, A.; Katz, H.E. Simultaneous increase in Seebeck coefficient and conductivity in a doped poly(alkylthiophene) blend with defined density of states. *Macromolecules*. **2010**, 43, 2897-2903.

[32] Mochalov, L.A.; Kuznetsov, Yu.M.; Dorokhin, M.V.; Fukina, D.G.; Knyazev, A.V.; Kudryashov, M.A.; Kudryashova, Yu.P.; Logunov, A.A.; Mukhina, O.V.; Zdoroveyshchev, A.V.; Zdoroveyshchev, D.A. Thermoelectrical properties of ternary lead chalcogenide plumbum-selenium-tellurium thin films with excess of tellurium prepared by plasma-chemical vapor deposition. *Thin Solid Films*. **2020**, 752, 139244-12.

[33] Chen, X.; Zhou, Z.; Lin, Y-H.; Nan, C. Thermoelectric thin films: Promising strategies and related mechanism on boosting energy conversion performance. *J. mater*. **2020**, 6, 494-512.

 doi:10.20944/preprints202305.0016.v1

[34] Ibanez, M.; Zamani, R.; Gorsse, S.; Fan, J.; Ortega, S.; Cadavid, D.; Morante, J.R.; Arbiol, J.; Cabot, A. Core-shell nanoparticles as building blocks for the bottom-up production of functional nanocomposites: PbTe-PbS thermoelectric properties. *ACS Nano*. **2013**, 7, 2573-2586.

[35] Othman, M.S. Mechanical response of PbSSe, PbSTe ternary and PbSnSTe quaternary alloys at high pressure. *ARO-sci. j. Koya univ*. **2020**, 8, 29-33.

[36] Dorokhin, M.V.; Kuznetsov, Yu.M.; Demina, P.B.; Erofeeva, I.V.; Zavrazhnov, A.Yu.; Boldin, M.S.; Lantsev, E.A.; Popov, A.A.; Boryakov, A.V.; Zdoroveyshchev, A.V.; Ved, M.V.; Zdoroveyshchev, D.A.; Korotkova, M.G. High-efficiency spark plasma sintered $Ge_{0.3}Si_{0.7}$:P thermoelectric energy converters with silicone phosphide as a source of phosphorus doping. *Nanoscale microscale thermophys. eng.* **2023**, 27, 125-134.